



An elastase activity reporter for Electronic Paramagnetic Resonance (EPR) and Overhauser-enhanced Magnetic Resonance Imaging (OMRI) as a line-shifting nitroxide

Natacha Jugniot, Indranil Duttagupta, Angelique Rivot, Philippe Massot, Colleen Cardiet, Anne Pizzoccaro, Marion Jean, Nicolas Vanthuyne, Jean-Michel Franconi, Pierre Voisin, et al.

► To cite this version:

Natacha Jugniot, Indranil Duttagupta, Angelique Rivot, Philippe Massot, Colleen Cardiet, et al.. An elastase activity reporter for Electronic Paramagnetic Resonance (EPR) and Overhauser-enhanced Magnetic Resonance Imaging (OMRI) as a line-shifting nitroxide. *Free Radical Biology and Medicine*, 2018, 126, pp.101–112. 10.1016/j.freeradbiomed.2018.08.006 . hal-02091886

HAL Id: hal-02091886

<https://amu.hal.science/hal-02091886>

Submitted on 7 Apr 2019

HAL is a multi-disciplinary open access archive for the deposit and dissemination of scientific research documents, whether they are published or not. The documents may come from teaching and research institutions in France or abroad, or from public or private research centers.

L'archive ouverte pluridisciplinaire **HAL**, est destinée au dépôt et à la diffusion de documents scientifiques de niveau recherche, publiés ou non, émanant des établissements d'enseignement et de recherche français ou étrangers, des laboratoires publics ou privés.

An elastase activity reporter for Electronic Paramagnetic Resonance (EPR) and Overhauser-enhanced Magnetic Resonance Imaging (OMRI) as a line-shifting nitroxide

Natacha Jugniot^{a,1}, Indranil Duttgupta^{b,1}, Angélique Rivot^a, Philippe Massot^a, Colleen Cardiet^a, Anne Pizzoccaro^c, Marion Jean^d, Nicolas Vanthuyne^d, Jean-Michel Franconi^a, Pierre Voisin^a, Gilles Devouassoux^c, Elodie Parzy^a, Eric Thiaudiere^a, Sylvain R.A. Marque^{b,e}, Abderrazzak Bentaher^c, Gérard Audran^b, Philippe Mellet^{a,f,*}

^a Centre de Résonance Magnétique des Systèmes Biologiques, UMR5536, CNRS, Université de Bordeaux, F-33076 Bordeaux, France

^b Aix Marseille Univ., CNRS, ICR, UMR 7273, case 551, Avenue Escadrille Normandie-Niemen, 13397 Marseille Cedex 20, France

^c Equipe "Inflammation et Immunité de l'Épithélium Respiratoire" - EA7426 Faculté de Médecine Lyon Sud, 165, Chemin du Grand Revoyet, 69495 Pierre Bénite, France

^d Aix Marseille Univ., CNRS, Centrale Marseille, iSm2, Marseille, France

^e Vorozhtsov Novosibirsk Institute of Organic Chemistry SB RAS, Pr. Lavrentjeva 9, 630090 Novosibirsk, Russia

^f INSERM, 33076 Bordeaux Cedex, France

ABSTRACT

Pulmonary inflammatory diseases are a major burden worldwide. They have in common an influx of neutrophils. Neutrophils secrete unchecked proteases at inflammation sites consequently leading to a protease/inhibitor imbalance. Among these proteases, neutrophil elastase is responsible for the degradation of the lung structure via elastin fragmentation. Therefore, monitoring the protease/inhibitor status in lungs non-invasively would be an important diagnostic tool.

Herein we present the synthesis of a MeO-Suc-(Ala)₂-Pro-Val-nitroxide, a line-shifting elastase activity probe suitable for Electron Paramagnetic Resonance spectroscopy (EPR) and Overhauser-enhanced Magnetic Resonance Imaging (OMRI). It is a fast and sensitive neutrophil elastase substrate with $K_m = 15 \pm 2.9 \mu\text{M}$, $k_{cat}/K_m = 930,000 \text{ s}^{-1} \text{ M}^{-1}$ and $K_m = 25 \pm 5.4 \mu\text{M}$, $k_{cat}/K_m = 640,000 \text{ s}^{-1} \text{ M}^{-1}$ for the *R* and *S* isomers, respectively. These properties are suitable to detect accurately concentrations of neutrophil elastase as low as 1 nM. The substrate was assessed with broncho-alveolar lavages samples derived from a mouse model of *Pseudomonas* pneumonia. Using EPR spectroscopy we observed a clear-cut difference between wild type animals and animals deficient in neutrophil elastase or deprived of neutrophil Elastase, Cathepsin G and Proteinase 3 or non-infected animals.

These results provide new preclinical *ex vivo* and *in vivo* diagnostic methods. They can lead to clinical methods to promote in time lung protection.

1. Introduction

Pulmonary inflammatory diseases represent a major health concern worldwide as well as an economic burden. They include asthma, cystic fibrosis (CF), chronic obstructive pulmonary disorder (COPD) (e.g., emphysema), acute respiratory distress syndrome and alpha-1-antitrypsin deficiency. For instance, COPD alone concerns a population estimated to 175 million people and accounts for 3.2 million deaths

ranking it to the fifth cause of mortality worldwide [1]. Among the precipitating factors for disease development are tobacco smoking, urban air pollution and wood fire smoke. A common denominator of pulmonary inflammatory diseases is the high neutrophil influx as seen in CF or during the exacerbation phase of COPD. At inflammation sites, neutrophils discharge four serine proteases into the extracellular environment whose concentrations surpass that of their corresponding physiologic inhibitors resulting in protease/anti-protease imbalance

* Corresponding author.

E-mail addresses: eric.thiaudiere@rmsb.u-bordeaux.fr (E. Thiaudiere), sylvain.marque@univ-amu.fr (S.R.A. Marque), azzak.bentaher@inserm.fr (A. Bentaher), g.audran@univ-amu.fr (G. Audran), philippe.mellet@rmsb.u-bordeaux.fr (P. Mellet).

causing tissue damage, hence progressive loss of lung functions.

Neutrophil elastase (NE), a potent protease, was shown to be the main tissue-destructive actor because of its large repertoire of substrate including structural proteins particularly elastin [2,3], a major lung structural protein, although the four neutrophil proteases can act synergistically [4].

Therapeutically, lungs protection needs an adapted treatment with protease inhibitors. However, preclinical research to setup such protocols is impaired by the absence of a reliable imaging method to localize deleterious enzyme activities in order to assess the actual protease/antiprotease balance status before and after treatment. Ultimately, an elastase activity imaging method valid for humans would detect lung inflammation long before any irreversible tissue damage could occur. Thus a treatment with inhibitors [5] or a change in habits could be proposed “in time” to save the lungs.

Molecular imaging of the proteolytic activity is most easily done using internally quenched fluorescent substrates. These substrates have good enzymatic constants because they can encompass both the P and P' regions in the Schechter and Berger nomenclature [6]. There are however several drawbacks of this method: substrate fluorescence quenching is not complete thus causing long waiting times to eliminate nonspecific “blinding” light, light tissue penetration is limited and prevents imaging of deeply seated tissues or skull and three-dimensional images are obtained by reconstruction.

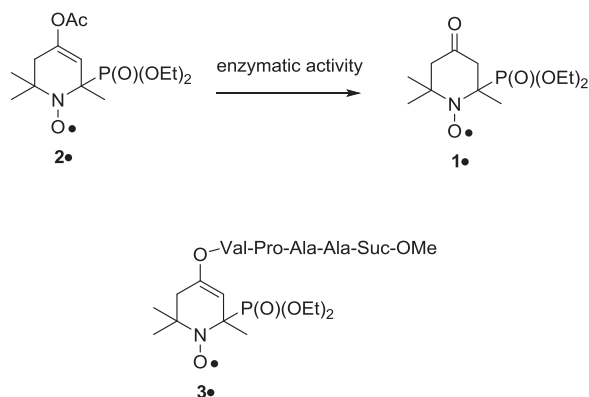
Magnetic Resonance Imaging (MRI) methods have a superior true 3D space encoding and use wavelengths that only weakly interfere with tissues. Electronic Paramagnetic Resonance (EPR) is a sensitive free radical detection method suitable in visible light-opaque media. Stable free radicals such as nitroxides or trityls can be detected or imaged in vitro and in vivo. Since unpaired electrons are particularly sensitive to the electronic environment some have been designed to display resonance line broadening or shifting to detect various parameters. Hence free radicals have been used for oximetry [7,8], redox status imaging [9,10], pH measurement [11–14], water content measurement [15] or to report on enzymatic activity [16–18]. EPR imaging (EPRI) can be used with these free radicals. Unfortunately, due to the very fast relaxation of free electrons EPRI still remains slow and insufficiently resolved. Magnetic Resonance Imaging (MRI) is the method of choice to deliver exquisite anatomical details but its low sensitivity so far prevented molecular imaging such as enzyme activity imaging. Interestingly, a line shifting substrate can also be monitored by Overhauser-enhanced Magnetic Resonance Imaging (OMRI). OMRI is an emerging imaging method designed to enhance NMR sensitivity. It is a double resonance experiment transferring a part of the higher spin polarization of an unpaired electron to the environing water protons (through the electron-proton Overhauser effect) which enhances the MRI signal that appears brighter [19].

It has been shown recently that OMRI at 0.2 T was able to reveal brain tumors in mice models of glioma through intravenous injection of a nonspecific nitroxide with high contrast on three-dimensional images [20]. Moreover, a nonspecific prototype of the line-shifting nitroxide later described in this study was able to reveal stomach and intestinal enzymatic activity [18] (see reaction in Scheme 1). Both studies showed that high contrast and high resolution images are possible in mice with short recording times.

In this paper the synthesis of MeO-Suc-(Ala)₂-Pro-Val-nitroxide (molecule 3• in Scheme 1), the first of a new family of dedicated protease substrates based on line-shifting nitroxides is reported. Its catalytic properties with neutrophil elastase and various enzymes were studied using EPR spectroscopy.

The substrate was probed in broncho-alveolar lavages from a mouse model of *Pseudomonas aeruginosa* lung infection with wild type and several mice knocked-out for neutrophil serine proteases.

It is also shown that this substrate is suitable for Overhauser-enhanced Magnetic Resonance Imaging.



Scheme 1. Enzymatic activity on enol acetate 2• releasing 1•. Elastase targeting substrate 3•.

2. Material and methods

2.1. Organic synthesis

2.1.1. General remarks

¹H nuclear magnetic resonance (NMR) spectra were recorded using an internal deuterium lock at ambient temperatures on the following instruments: Bruker AC 400 (400 MHz) and Bruker AC 300 (300 MHz). Data are presented as follows: chemical shift (in ppm), integration, multiplicity (*s* = singlet, *d* = doublet, *t* = triplet, *m* = multiplet, *br* = broad, *dd* = doublet of doublets), coupling constant (*J* in Hz) and integration. ³¹P NMR spectra were recorded on a Bruker AC 300 (122 MHz) and on a Bruker AC 400 (162 MHz) spectrometers with complete proton decoupling. Chemical shifts (δ) were reported in ppm using TMS as internal reference for ¹H and ¹³C NMR spectra, and 85% H₃PO₄ for ³¹P NMR spectra. High-resolution mass spectra (HRMS) were performed on a SYNAPT G2 HDMS (Waters) spectrometer equipped with atmospheric pressure ionization source (API) pneumatically assisted. Samples were ionized by positive electrospray mode as follows: electrospray tension (ISV): 2800 V; opening tension (OR): 20 V; nebulization gas pressure (nitrogen): 800 L/h. Low resolution mass spectra were recorded on ion trap AB SCIEX 3200 QTRAP equipped with an electrospray source. The parent ion (*M*⁺, [*M* + *H*]⁺, [*M* + *Na*]⁺ or [*M* + *NH*]⁺) is quoted. Analytical thin layer chromatographies (TLC) were carried out on Merck Kieselgel 60 F254 plates. Flash column chromatographies were carried out on Merck Kieselgel 60 (230–400 mesh). Solvent system: gradients of DCM/MeOH; EtOAc/EtOH. All experiments were performed under anhydrous conditions and an inert atmosphere of argon and, except where stated, using dried apparatus and employing standard techniques for handling air-sensitive materials. For EPR measurements, samples with 0.5 mM concentration of nitroxide were prepared in non-degassed solvents. Experiments were performed indifferently on Elexsys, EMX or ER 100D Bruker machines (a difference smaller than 0.1 G was noticed). EPR spectra were recorded with a gain of 2 105 (72 dB for Elexsys), a modulation amplitude of 1.0 G, a sweep width of 150 G, a sweep time of 21 s, and a power of 20 mW.

2.1.2. (9H-fluoren-9-yl)methyl-(S)-2-(((S)-1-(benzyloxy)-3-methyl-1-oxobutan-2-yl)carbamoyl) pyrrolidine-1-carboxylate (2)

DIPEA (2 mL, 11.5 mmol) was added dropwise to a stirred suspension of L-Val-OBn-HCl (2.8 g, 11.5 mmol) in dichloromethane (30 mL) at room temperature under an atmosphere of nitrogen. On dissolution, the solution was cooled to 0 °C and Fmoc-L-Pro (4.26 g, 12.6 mmol) and 1-hydroxybenzotriazole (1.86 g, 13.8 mmol) were added successively, each in one portion. The suspension was stirred at 0 °C for a further 15 min, and then DCC (2.85 g, 13.8 mmol) was added in one portion. The mixture was allowed to warm to room temperature over the course

of 18 h and then filtered, and the filtrate was evaporated in vacuo. The residue was taken up in ethyl acetate and filtered, and the filtrate was then washed with 10% aqueous citric acid solution followed by saturated aqueous sodium bicarbonate solution. The combined organic layers were dried and evaporated in vacuo to afford the crude product which was purified by chromatography on silica using 3:2 petroleum ether–EtOAc as eluent to yield the protected dipeptide **2** (5.94 g, 11.28 mmol) as a light yellow solid (98%). $[\alpha]_D^{20} - 50$ (c 1.0, CHCl₃). ¹H NMR (300 MHz, CDCl₃) δ 7.68 (d, $J = 7.5$ Hz, 2H), 7.48 (s, 2H), 7.33–7.17 (m, 9.7H), 6.43 (br s, 0.3H), 5.20–4.82 (br m, 2H), 4.48–4.16 (m, 5H), 3.48–3.38 (m, 2H), 2.27–1.86 (m, 5H), 0.80 (d, $J = 6.8$ Hz, 2H), 0.75 (d, $J = 6.6$ Hz, 1H). ¹³C NMR (75 MHz, CDCl₃) δ 172.2, 171.6, 156.1, 155.2, 143.8, 141.3, 135.5, 128.6, 128.4, 128.3, 127.8, 127.1, 125.1, 120.0, 67.8, 67.0, 61.2, 60.4, 57.3, 56.7, 53.5, 47.6, 47.2, 47.0, 33.9, 31.5, 31.2, 28.2, 24.7, 23.7, 19.1, 17.6. HRMS (ESI) calc for C₃₂H₃₅N₂O₅⁺: 527.2540 [M+H]⁺; found: 527.2547.

2.1.3. (((9H-fluoren-9-yl)methoxy)carbonyl)-L-prolyl-L-valine (**3**)

To a solution of **2** (5.94 g, 11.28 mmol) in MeOH (80 mL) was added 10% Pd/C (600 mg), and the mixture was stirred for 10 h in hydrogen atmosphere (1 atm). The reaction mixture was filtered through Celite, and MeOH removed in vacuo to afford the fmoc protected dipeptide **3** in quantitative yield (4.92 g, 11.27 mmol). $[\alpha]_D^{20} - 46.1$ (c 1.0, CHCl₃). ¹H NMR (300 MHz, CDCl₃) δ 7.65–7.12 (m, 8.7H), 6.52 (br s, 0.3H), 4.15–4.38 (br m, 5H), 3.41 (br m, 2H), 2.20–1.83 (m, 5H), 0.84–0.78 (m, 6H). ¹³C NMR (75 MHz, CDCl₃) δ 174.7, 172.1156.1, 155.6, 149.0, 143.9, 143.7, 141.3, 140.5, 127.7, 127.1, 126.9, 125.1, 124.0, 120.0, 119.8, 68.2, 67.9, 61.0, 60.4, 57.2, 56.7, 53.5, 47.5, 47.1, 42.4, 31.2, 31.0, 28.5, 24.6, 23.5, 19.1, 17.5. HRMS (ESI) calc for C₂₅H₂₉N₂O₅⁺: 437.2071 [M+H]⁺; found: 437.2073.

2.1.4. (S)-2-((S)-1-(((9H-fluoren-9-yl)methoxy)carbonyl)pyrrolidine-2-carboxamido)-3-methyl-butanoic pivalic anhydride (**4**)

To an ice cold solution of dipeptide **3** (1.23 g, 2.83 mmol) in 3 mL dry dichloromethane, Pivaloyl chloride (0.7 mL, 5.7 mmol) was added followed by the dropwise addition of triethyl amine (0.6 mL, 4.3 mmol). The reaction mixture was then allowed to stir at 0 °C for 1 h (TLC shows completion of reaction) after which excess dichloromethane was removed and the residue was taken up in diethyl ether. The solution was then filtered through a celite bed. Removal of diethyl ether in vacuo yielded the targeted anhydride **4** as a white foamy solid in a quantitative yield which was used in the next reaction without any further purification.

2.1.5. Methyl (S)-4-((1-(benzyloxy)-1-oxopropan-2-yl)amino)-4-oxobutanoate (**6**)

DIPEA (17 mL, 17 mmol) was added dropwise to a stirred suspension of L-Ala-OBn-HCl (6.02 g, 27.9 mmol) in dichloromethane (70 mL) at room temperature under an atmosphere of nitrogen. On dissolution, the solution was cooled to 0 °C and succinic acid monomethyl ester (4.05 g, 30.7 mmol) and 1-hydroxybenzotriazole (4.52 g, 33.48 mmol) were added successively, each in one portion. The suspension was stirred at 0 °C for a further 15 min, and then DCC (6.91 g, 33.48 mmol) was added in one portion. The mixture was warmed to room temperature in 18 h and then filtered, and the filtrate was evaporated in vacuo. The residue was taken up in ethyl acetate and filtered, and the filtrate was then washed with 10% aqueous citric acid solution followed by saturated aqueous sodium bicarbonate solution. The combined organic layers were dried and evaporated in vacuo to afford the crude product which was purified by chromatography on silica using 3:2 petroleum ether–EtOAc as eluent to yield **6** (7.2 g, 24.55 mmol, 88%) as a white solid. $[\alpha]_D^{20} - 4.3$ (c 1.0, CHCl₃). ¹H NMR (300 MHz, CDCl₃) δ 7.30–7.20 (m, 5H), 6.36 (s, 1H), 5.08 (dd, $J = 18, 12$ Hz, 2H), 4.54 (p, $J = 7.2$ Hz, 1H), 3.58 (s, 1H), 2.66–2.54 (m, 2H), 2.50–2.4 (m, 2H), 1.32 (d, $J = 7.2$ Hz, 1H). ¹³C NMR (75 MHz, CDCl₃) δ 173.3, 172.9, 171.0, 135.4, 128.6, 128.4, 128.1, 67.1, 51.8, 48.2, 30.8, 29.2, 18.3. HRMS

(ESI) calc for C₁₅H₂₀NO₅⁺: 294.1336 [M+H]⁺; found: 294.1340.

2.1.6. Methyl 4-(((S)-1-(((S)-1-(benzyloxy)-1-oxopropan-2-yl)amino)-1-oxopropan-2-yl)amino)-4-oxobutanoate (**7**)

To a solution of **6** (7 g, 23.86 mmol) in MeOH (80 mL) was added 10% Pd/C (700 mg), and the mixture was stirred for 10 h in hydrogen atmosphere (1 atm). The reaction mixture was filtered through Celite followed by MeOH removal in vacuo to yield quantitatively the free acid (4.85 g, 23.8 mmol).

DIPEA (14.9 mL, 83.52 mmol) was added dropwise to a stirred suspension of L-Ala-OBn-HCl (6.16 g, 28.56 mmol) in dichloromethane (100 mL) at room temperature under an atmosphere of nitrogen. On dissolution, the solution was cooled to 0 °C and the acid obtained in the previous step (4.85 g, 23.8 mmol) and 1-hydroxybenzotriazole (3.86 g, 28.56 mmol) were added successively, each in one portion. The suspension was stirred at 0 °C for a further 15 min, and then DCC (5.89 g, 28.56 mmol) was added in one portion. The mixture was warmed to room temperature in 18 h and then filtered, and the filtrate was evaporated in vacuo. The residue was taken up in ethyl acetate and filtered, and the filtrate was then washed with 10% aqueous citric acid solution followed by saturated aqueous sodium bicarbonate solution. The combined organic layers were dried and evaporated in vacuo to leave the crude product which was purified by chromatography on silica using 3:2 petroleum ether–EtOAc as eluent to afford **7** (7.5 g, 20.71 mmol) as a white solid in 87% yield. $[\alpha]_D^{20} - 44$ (c 1.0, CHCl₃). ¹H NMR (300 MHz, CDCl₃) δ 7.25 (s, 5H), 7.10 (s, 1H), 6.69 (s, 1H), 5.07 (dd, $J = 18, 12$ Hz, 2H), 4.58–4.42 (m, 2H), 3.55 (s, 3H), 2.57 (dd, $J = 10.0, 4.0$ Hz, 2H), 2.41 (dd, $J = 10.4, 4.5$ Hz, 2H), 1.32 (d, $J = 7.2$ Hz, 3H), 1.27 (d, $J = 7.0$ Hz, 3H). ¹³C NMR (75 MHz, CDCl₃) δ 173.4, 172.4, 172.2, 171.3, 135.5, 128.6, 128.4, 128.1, 67.0, 51.8, 48.8, 48.2, 30.8, 29.2, 18.4, 17.8. HRMS (ESI) calc for C₁₈H₂₅N₂O₆⁺: 365.1707 [M+H]⁺; found: 365.1696.

2.1.7. Methyl-4-(((S)-1-(((S)-1-((2,5-dioxypyrrolidin-1-yl)oxy)-1-oxopropan-2-yl)amino)-1-oxo-propan-2-yl)amino)-4-oxobutanoate (**8**)

To a solution of **7** (7.5 g, 20.71 mmol) in MeOH (80 mL) was added 10% Pd/C (750 mg), and the mixture was stirred for 10 h in hydrogen atmosphere (1 atm). The reaction mixture was filtered through celite followed by MeOH removal in vacuo to yield quantitatively the free acid (5.68 g, 20.71 mmol). $[\alpha]_D^{20} + 8.7$ (c 1.0, CHCl₃). ¹H NMR (300 MHz, MeOD) δ 4.39 (qd, $J = 7.1, 3.1$ Hz, 2H), 3.66 (s, 3H), 2.64 (dd, $J = 10.1, 4.0$ Hz, 2H), 2.52 (dd, $J = 10.3, 4.0$ Hz, 2H), 1.41 (d, $J = 7.3$ Hz, 3H), 1.35 (d, $J = 7.2$ Hz, 3H). ¹³C NMR (75 MHz, MeOD) δ 175.7, 174.9, 174.7, 174.0, 52.2, 50.1, 49.2, 31.2, 30.0, 18.0, 17.6. HRMS (ESI) calc for C₁₁H₁₉N₂O₆⁺: 275.1238 [M+H]⁺; found: 275.1237.

To a solution of the free acid from above (484 mg, 1.76 mmol) and N-Hydroxysuccinimide (203 mg, 1.76 mmol) in 7 mL THF, DCC (364 mg, 1.76 mmol) was added in one portion. The mixture was stirred at room temperature for 18 h and then filtered, and the filtrate was evaporated in vacuo to afford the NHS ester **8** as a white solid in quantitative yield (650 mg, 1.75 mmol) which was used in the next reaction without further purification. HRMS (ESI) calc for C₁₅H₂₂N₃O₈⁺: 372.1401 [M+H]⁺; found: 372.1400.

2.1.8. Synthesis of R-4•

A solution of ketone **R-1•** (209 mg, 0.71 mmol) in dry THF (10 mL) was slowly added to solution of LiHMDS (1.0 M solution in THF, 1.2 mL, 1.21 mmol, 1.70 equiv.) at 78 °C in dry THF (5 mL). The mixture was stirred for 3 h from –78 °C to –45 °C. Then, **4** (739 mg, 1.42 mmol, 2 equiv.) was slowly added as a cold (–45 °C) solution in 10 mL THF. The mixture was stirred for 2.5 h, then it was poured quenched with saturated aqueous NH₄Cl solution and extracted with EtOAc. The combined organic extracts were dried with MgSO₄, filtered, and concentrated under vacuo. Column chromatography of the residue gave starting material **R-1•** (92 mg, 0.31 mmol) and the targeted product **R-4•**

(175 mg, 0.25 mmol, 65% based on recovered starting material) as a red foamy solid. HRMS (ESI) calc for $C_{36}H_{42}N_2O_8PNa^+$: 728.3545 $[M + Na]^+$; found: 728.3553, $[\alpha]_D^{20} - 58.3$ (c 1.0, $CHCl_3$). EPR (CH_2Cl_2): a_N 14.9 G, a_P 39.0 G.

2.1.9. Synthesis of S-4•

S-4• was prepared following the same procedure as that for R-4•. Yield 229 mg, 0.32 mmol, 91% based on recovered starting material as a red foamy solid from S-1• (208 mg, 0.71 mmol), recovered starting material S-1• 105 mg, 0.36 mmol. HRMS (ESI) calc for $C_{36}H_{42}N_2O_8PNa^+$: 728.3545 $[M + Na]^+$; found: 728.3553, $[\alpha]_D^{20} - 21.3$ (c 1.0, $CHCl_3$). EPR (CH_2Cl_2): a_N 15.2 G, a_P 39.10 G.

2.1.10. Synthesis of R-5•

To a solution of R-4• (275 mg, 0.39 mmol) in 20 mL DCM at 0 °C, DBU (69 μ L, 0.46 mmol) was added. The reaction mixture was stirred at 0 °C for 3 h (TLC showed completion of reaction) followed by column purification to yield the deprotected R-4• in 74% yield (143 mg, 0.29 mmol).

Deprotected R-4• (143 mg, 0.29 mmol) and **8** (120 mg, 0.32 mmol) was dissolved in 5 mL anhydrous DMF and the mixture was allowed to stir for 18 h at room temperature. Removal of DMF *in vacuo* followed by column chromatography yielded R-5• in 34% overall yield (105 mg, 0.14 mmol). HRMS (ESI) calc for $C_{33}H_{56}N_5O_{12}P^+$: 745.3658 $[M + H]^+$; found: 745.3662. EPR (CH_2Cl_2): a_N 15.0 G, a_P 38.9 G.

2.1.11. Synthesis of S-5•

Similar procedure as that of above was used for the synthesis of R-5•, from S-4• (186 mg, 0.26 mmol) yielded the final product S-2• in 50% overall yield (52 mg, 0.07 mmol). HRMS (ESI) calc for $C_{33}H_{56}N_5O_{12}P^+$: 745.3658 $[M + H]^+$; found: 745.3659. EPR (CH_2Cl_2): a_N 15.0 G, a_P 39.0 G.

2.2. Enzymes

Neutrophil Elastase, Porcine Pancreatic Elastase, Proteinase 3 and Cathepsin G were purchased from Elastin Products Company (Missouri, USA). Bovine chymotrypsin and trypsin-TPCK treated were from Worthington (New Jersey, USA). Matrix Metallo Proteinases -2, -7 and -9 were purchased from Calbiochem. Stock enzyme solutions were prepared at about 10^{-5} M in buffer HEPES 50 mM, 0.15 M NaCl, pH 5, stored at -20 °C and later titrated as described under. All experiments were done in HEPES buffer 50 mM pH 7.4, 0.15 M NaCl and IGEPAL 0.05%.

2.2.1. Enzymes titration

Enzyme's active sites in solution were quantified by spectrophotometric titration using synthetic chromogenic reagents which combined stoichiometrically with active sites (1:1). Chromogenic reagents: Succinyl-Ala-Ala-pro-phe-p-nitroanilide (Cathepsin G, chymotrypsin), MeO-succinyl-Ala-Ala-Pro-Val-p-nitroanilide (NE, Proteinase 3) (Elastin Products Company, USA), z-Phe-Arg-p-nitroanilide (trypsin-TPCK) and Succinyl-Ala-Ala-Ala-p-nitroanilide (PPE) (BACHEM, Switzerland) were prepared in dimethyl sulfoxide (DMSO). Trasylol from bovine lung, trypsin inhibitor from soybean (SIGMA) and Eglin C from leech (gift from Dr. H. P. Schnebli, Ciba-Geigy, Basel, Switzerland), natural protease inhibitors, were dissolved in HEPES buffer. Titrations of NE, PPE, proteinase 3 and cathepsin G were made with Eglin C, titrations of chymotrypsin and trypsin-TPCK were made with trasylol and trypsin inhibitor from soybean respectively. Activity of inhibitors was assumed to be 100%. MMP-2,-7,-9 were all active on the fluorescent substrate Dnp-Pro-Leu-Gly-Leu-Trp-Ala-D-Arg-NH₂ (Bachem). Their concentration was inferred from the manufacturer specifications.

2.3. EPR spectroscopy of peptide-nitroxide substrates

All samples were loaded in 75 μ L (75 mm) capillaries (BLAUBRAND micropipettes). Acquisitions were performed at 25 °C with a temperature controller (BIO-I, NOXYGEN, Germany) fitted to an EMXnano EPR spectrometer (BRUKER, Germany), under the control of Xenon software (BRUKER). Quantitation of substrate and product nitroxides at each time of the kinetics was done by fitting with both reference spectra using the Spinfit module of Xenon software. Substrate and product concentrations were obtained using the included Spincount calibrated module.

Enzymatic activity assays were carried out using the EPR spectroscopy to monitor the substrate hydrolysis.

2.3.1. Enzymatic specificity screening *in vitro*

A list of proteases, described in Enzymes section, with various specificities and origins was tested in pursuit of an effective proteolytic activity on the nitroxide. All experiments were done with 1 nM proteases. Enzymatic reactions were initiated by adding a small volume of substrate 25 μ M. Kinetics was immediately recorded by EPR during 2 h. EPR acquisition parameters were set as follows: $B_0 = 3423$ G, sweep width = 120 G; sweep time = 10 s, attenuation = 6 dB; delay between scan = 30 s; modulation amplitude = 1 G; gain = 50 dB. Post processing was done with IGOR Pro (Wavemetrics, Lake-Oswego, OR, USA), initial velocities from different enzymes were collected and compared in a histogram.

2.3.2. Michaelis kinetics constants of NE with both peptide-nitroxide isomers

Kinetic reactions were made with NE 1 nM by adding a range of 11 concentrations of substrate from 2.5 μ M to 200 μ M, prepared contemporaneously to limit spontaneous hydrolysis. EPR acquisition parameters were set as follows: $B_0 = 3423$ G, sweep width = 120 G; sweep time = 10 s, attenuation = 6 dB; delay between scan = 30 s; modulation amplitude = 4 G; gain = 50 dB. Thus spectra were recorded at 10 s interval. Quantitation of substrate and product nitroxides at each time of the kinetics was done by fitting with both reference spectra using the Spinfit module of Xenon software. Substrate and product concentrations were calculated using the included Spincount calibrated module. Product concentrations were plotted as a function of time. Initial velocities were extracted by linear regression on the linear portion of the plot (less than 5% of substrate consumed) for each initial substrate concentration. Initial velocities values were finally plotted versus substrate concentration. Michaelis-Menten hyperbolic representation was built from the initial velocities and a nonlinear regression analysis was performed using Michaelis-Menten equation: $V_0 = \frac{k_{cat} \times [E_0] \times [S_0]}{K_m + [S_0]}$. Enzymatic parameters, K_m and k_{cat} were determined for both substrate isomers.

2.3.3. Neutrophil elastase activity in broncho alveolar lavage

Proteolysis was started by adding 1 mM substrate in 30 μ L of broncho alveolar lavage (BAL) samples. Samples were then immediately loaded in capillaries. EPR acquisition parameters were set as follows: $B_0 = 3423$ G, sweep width = 120 G; sweep time = 10 s, attenuation = 25 dB; delay between scan = 30 s; modulation amplitude = 1 G; gain = 40 dB. Kinetic reactions were followed for 8 h at 25 °C. All experiments were repeated on 4 or 5 different mice. The resulting slope of progress curves $[Product] = f(time)$ were plotted against the various genotypes in a histogram representation. Results were normalized with the condition WT infected.

2.4. Mouse inflammation model

2.4.1. Generation of mice deficient in CG, NE, and PR3

Simultaneous deficiency of the *Prtn3* and *Ela2* gene cluster (129S6/

SvEv), deficiency in CG(129S6/SvEv-C57BL/6J), and deficiency in NE (129S6/SvEv-C57BL/6J) were generated by targeted mutagenesis as described elsewhere [21–23]. NE-PR3-deficient mice and CG-deficient mice were crossbred to generate heterozygote-deficient progeny (F_1). The F_1 progeny were intercrossed to generate mice deficient in NE, PR3, and CG, referred to as NSP-KO [3]. Mouse strains were subsequently backcrossed (eight generations) on a pure C57BL6/J background. Mice were housed in a pathogen-free facility with food and water *ad libitum* and a 12-h light/dark cycle.

Animal handling and procedures were approved by the Animal Studies Committee at our institution (Health and Animal Protection Office, Châlons-en-Champagne, France, Authorisation number: 51–31) in accordance with the guidelines of the Federation of European Laboratory Animal Science Associations and following the European Directive 2010/63/EU on the protection of animals used in scientific procedures.

2.4.2. Bacteria and intranasal infection

P. aeruginosa H103 was kindly provided by Dr. Hancock (Vancouver, BC, Canada) [24]. An overnight bacterial culture (1 mL) was grown in Luria Bertani broth (10 mL) at 37 °C to late exponential phase (3 h). Bacteria were washed twice with PBS (pH 7.4) and the optical density (OD) of the cultures was determined at 600 nm ($1 \text{ OD}_{600 \text{ nm}} \approx 1 \times 10^9 \text{ bacteria/mL}$).

Mice ($n = 5$ mice/genotype) were challenged intranasally with bacteria and sacrificed at fixed time points. Briefly, mice were anesthetized by intraperitoneal (intraperitoneal) injection of ketamine hydrochloride (75 mg/kg) and medetomidine hydrochloride (1 mg/kg). Next, mice were challenged intranasally with 50 μL of saline buffer (PBS) containing a predetermined sublethal dose of bacteria (10^6 CFUs /per mouse) [25]. Control mice ($n = 5$ mice/genotype) were challenged with 50 μL of sterile PBS alone. WT mice, NE-KO deficient mice and NSP-KO mice were sacrificed at 24 h post-infection. At this time point, mouse lungs were analyzed for inflammatory cell recruitment and detection of free active NE. Of note, all types of mice displayed a morbid state that was more marked in KO mice after 24 h.

2.4.3. BAL collection

Mice were sacrificed, and the lungs were gently perfused with saline via the right ventricle. The trachea was exposed through a midline incision and was cannulated using a sterile 22-gauge catheter (BD Biosciences, Franklin Lakes, NJ). Lungs were lavaged *in situ* (BAL), with 1 mL of PBS, pH 7.4, cycled in three times. Identical recoveries of BAL (700 μL per mouse) were obtained for each mouse [26]. Total cell and differential counts were immediately performed on aliquots of BAL fluids. The remaining BALs were centrifuged, aliquoted, and stored in -80°C until use.

2.5. OMRI

2.5.1. EPR cavity and MRI system

The OMRI system used in all experiments is an EPR cavity (Bruker, Wissemburg, France) inserted at the center of Cirrus Open 0.2 T MRI system (MRI Tech, Canada). This permanent magnet at 0.193 T is operated at a proton frequency of 8.24 MHz and maximal field gradient strength was 20 mT/m in the three directions of space.

Electron spin saturation was carried out in the EPR cavity, which has a cylindrical geometry (240 mm diameter and 28 mm width). An opening (28 mm diameter) in the middle of the cavity enabled sample positioning. Its design and mode of operation, Transverse-Electric TE011 mode, was the focus of the development in order to minimize the impact of electromagnetic HF field [27] and to limit Eddy currents [17].

The HF amplification channel, including a synthesizer and two specific amplifiers (RFPA, Artigues-pres-Bordeaux, France), generated the HF wave. The EPR resonance frequency was around 5.4 GHz, according to the central EPR frequency of the nitroxide of interest. The

resonant cavity was tuned and matched with the help of a network analyzer (Agilent Technologies, Santa Clara, CA, USA) at this resonance frequency.

2.5.2. Pulse sequences

2D magnetic resonance images were generated with a Gradient Echo sequence. It was modified to include a continuous EPR saturation during all the acquisition which started 300 ms prior to the first NMR RF pulse. All MR adjustments were done manually, using the same fixed parameters: TE/TR = 20/200 ms, field of view $40 \times 40 \text{ mm}^2$, Matrix size 64×64 , flip angle 30° , receiver bandwidth 20 kHz, with and without HF irradiation (S_{ON} and S_{OFF}).

2.5.3. Overhauser enhancements and EPR frequency

The EPR irradiation frequency was adjusted on the 4th peak upfield of the EPR spectrum of the nitroxide to have a specific excitation of the nitroxide of interest. Frequency sweep experiments were carried out to characterize OMRI response of substrate and product at 1 mM each. The Overhauser enhancement was calculated as the ratio of the absolute value of the NMR signal-to-noise ratio (SNR) in the presence of electron saturation divided by the SNR measured without electron saturation (S_{OFF}).

The DNP factor (DNPF) is defined as $\langle I_z \rangle / I_0 - 1$ where $\langle I_z \rangle$ stands for the expected value of proton magnetization in the presence of EPR saturation and I_0 is the equilibrium proton magnetization. Assuming a steady-state electron saturation,

$$\text{DNPF} = (\rho f s / n) \gamma_S / \gamma_I, \quad (1)$$

where γ_S and γ_I are the electron and proton gyromagnetic ratio, respectively, ρ the electron-nucleus coupling factor, n the number of EPR lines, s the saturation factor and f the leakage factor. The leakage factor can be expressed as:

$$f = r_1 \cdot [c] / (R_{110} + r_1 \cdot [c]),$$

where $[c]$ is the nitroxide concentration, r_1 its longitudinal relaxivity and R_{110} is the proton longitudinal relaxation rate constant in the absence of nitroxide. Due to the negative sign of the electron gyromagnetic ratio and the positive sign of the coupling factor (mostly dipolar in liquids), the Overhauser effect induce an out-of-phase shift of the proton magnetization and thus a negatively signed DNPF. The relationship between the Overhauser enhancement and the DNPF is:

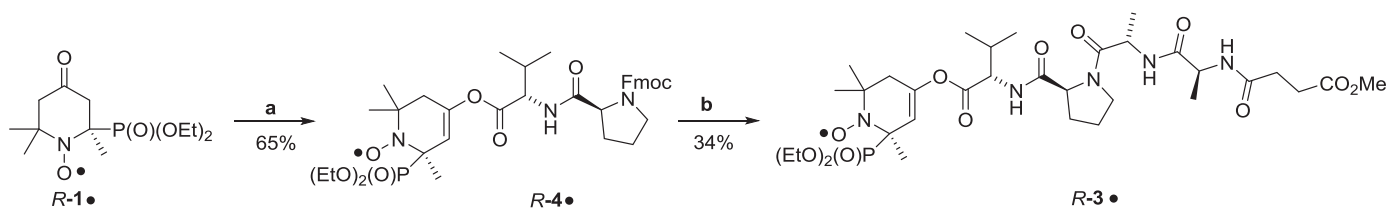
$$\text{Overhauser enhancement} = |\text{DNPF}| - 1$$

DNP factor vs nitroxide concentration were evaluated by curve fitting to Eq. (1) with $R_{110} = 0.4 \text{ s}^{-1}$ and r_1 (determined from inversion-recovery experiments) as fixed parameters, and the product $s \cdot \rho$ as a floating parameter.

Details on the theoretical background can be found in Overhauser [28], Abragam et al. [29] and a summary is given in Mellet et al. [27]. Overhauser enhancements were finally plotted against EPR frequency and specific irradiation frequency was selected for each nitroxide form (Fig. 6). Lineshape were evaluated from curve fit to a lorentzian function. Nitroxide relaxivity was calculated from inversion-recovery experiments [30]. Inversion times ranged from 10 ms to 10 s. NMR signals vs inversion delay were fitted to a single exponential recovery curve and relaxation rate constants vs nitroxide concentration (0–2 mM range) were adjusted with a linear model.

2.5.4. Kinetic measurements *in vitro*

OMRI of proteolysis kinetics was performed both by looking at the substrate consumption and by looking at the product formation in separate experiments. Experiments were done in the presence of 40 nM NE (product kinetic) and 20 nM NE (substrate kinetic). Kinetics of hydrolysis were started by adding 0.5 mM substrate (product formation) or 1 mM (substrate consumption). Control experiments were carried out without enzyme. For each nitroxide form, two sets of 2D images were



Scheme 2. Preparation of R-3•: (a) Reagents and conditions: a) LiHMDS, **4**, THF, -78 to -45 °C, 65%; b) (1) DBU, DCM, 0 °C, 3 h; (2) **8**, DMF, rt, 18 h, 34% for both steps 1 and 2.

acquired at various time intervals with and without electron saturation with the imaging parameters described above.

3. Results

3.1. Synthesis of the methoxy-succinyl-alanine-alanine-proline-valine-nitroxide enol ester

As mentioned above, nitroxides **1•/2•** exhibit high potential to investigate proteolysis both by EPR and OMRI. Recently, enantiomers of **1•** were separated, identified and, then used for the preparation of the peptide-nitroxide substrate (reported elsewhere [31]).

After applying a similar approach, (details of the synthesis modifications are published elsewhere [31]) peptide-nitroxides **R-3•** and **S-3•** putatively specific of neutrophil elastase protease were prepared in two steps (Scheme 2 and Material and Methods section), in the first step, the condensation of the activated peptide **4** (Scheme 3A and see Material and Methods section) with the enolate of **R-1•** to yield nitroxide **R-4•**, and, in the second step, coupling of **R-4•** with the activated peptide **8** (Scheme 3B) to afford **R-3•**. The same procedure was applied to **S-1•** to yield **S-3•** (overall yield of 45%, see Material and Methods section).

Activated peptides **4** and **8** were prepared according to conventional procedures (Scheme 3A and B, respectively). That is, using the standard DCC procedure Fmoc-protected L-proline **1** is coupled to benzyl-protected L-valine to afford dipeptide **2** in 98% yields. The latter is quantitatively debenzylated into dipeptide **3** which was transformed into activated anhydride **4** using pivaloyl chloride (Scheme 2A) [32,33]. The second fragment **8** was synthesized in 3 steps from Succinic acid monomethyl ester **5** and used without further purification. Using DCC coupling procedure, peptide **6** was prepared in 88% yield by coupling **5** with L-Ala-OBn.HCl. Debenzylation of **6** followed by coupling with L-Ala-OBn.HCl provided the benzyl protected dipeptide **7** in 87% yields. Dipeptide **7** was then deprotected and converted into its NHS ester **8** using N-hydroxy succinimide and DCC (Scheme 3B). [34] Crude **8** was used in the preparation of **R-3•** and **S-3•** without further purification.

3.2. Enzyme kinetics of substrate to product hydrolysis by NE

3.2.1. Enzymatic hydrolysis of the substrate

Chemical structures of substrate and enzymatic reaction product are illustrated in Scheme 4.

As a preliminary experiment, the kinetics of hydrolysis of the substrate by neutrophil elastase was studied by EPR (Fig. 1).

The EPR parameters including nitrogen and phosphorus hyperfine coupling constants (a_N and a_P respectively) as they appear before and after hydrolysis of substrate in the presence of NE are reported in Table 1.

Owing to the difference of 4.9 G in their a_P values, substrate and product spectra are sufficiently resolved to avoid peaks overlapping, thus allowing individual quantification in a substrate/product mixture.

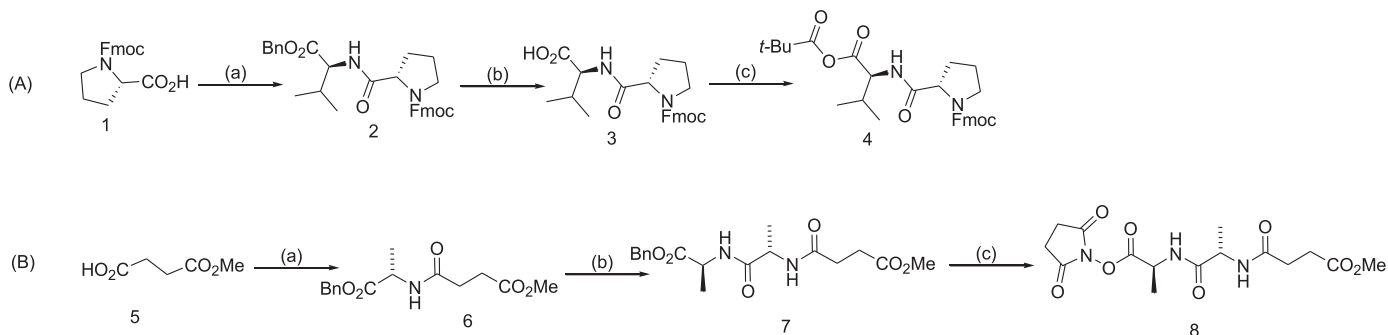
As described in Table 1, product's linewidth was 1.22 G while substrate's linewidth was 1.84 G. Thus, for EPR spectroscopy measurements the product will show a better sensitivity and for Overhauser-enhanced MRI specific excitation of the product will provide a greater signal enhancement compared to the substrate as outlined hereafter.

3.2.2. Determination of the Michaelis constants

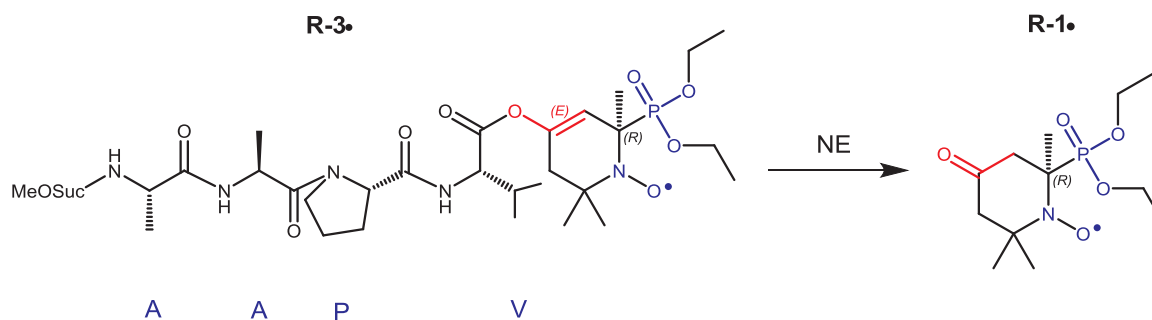
Kinetics of consumption of substrate and formation of product were monitored in the concentration range of 2.5–200 μ M (Fig. 2).

Initial velocities were deduced from the slope of the linear part of each progress curve displayed in Fig. 2. Finally, Michaelis-Menten plots (Fig. 3) allowed us to determine Michaelis constants (Table 2).

Kinetic constants for **R-3•** derived from these measurements are $K_m = 15$ μ M and $k_{cat} = 14$ s^{-1} , indicating a catalytic efficiency, k_{cat}/K_m , of 940 000 $s^{-1} M^{-1}$. Constants for **S-3•** are $K_m = 25$ μ M and $k_{cat} = 16$ s^{-1} , with k_{cat}/K_m , of 640 000 $s^{-1} M^{-1}$. Both isomers thus display similar kinetic constants, having a K_m 4–7 fold lower than that of the reference chromogenic substrate MeO-Suc-(Ala)₂-Pro-Val-pNA and a catalytic constant 6–9 fold higher [35]. These results suggest that better interactions occur with the P' part of the substrate, namely the nitroxide group, than with the widely used paranitroanilide leaving group, as the peptide that fills the P part was identical in the two substrates.



Scheme 3. Preparation of activated peptide 4 (A) and 8 (B). Reagents and conditions for (A): (a) L-Val-OBn, HOBT, DCC, DIPEA, DCM, 0 °C to rt, 18 h, 98%; (b) Pd/C, H_2 , MeOH, 10 h, rt, quantitative; (c) t -BuCOCl, Et_3N , 0 °C, 1 h; and for (B): (a) L-Ala-OBn.HCl, HOBT, DCC, DIPEA, DCM, 0 °C to rt, 18 h; (b) (1) Pd/C, H_2 , MeOH, 10 h, rt, (2) (a), 87% yield for both steps 1 and 2; (c) (1) Pd/C, H_2 , MeOH, 10 h, rt, (2) N-hydroxy succinimide, DCC, THF, rt, 18 h, quantitative yield for each step.



Scheme 4. Proteolysis reaction of MeO-Suc-(Ala)₂-Pro-Val-(R)nitroxide enol ester into the ketone form of the nitroxide and a free peptide by neutrophil elastase (NE). The reaction is the same with the isomer S.

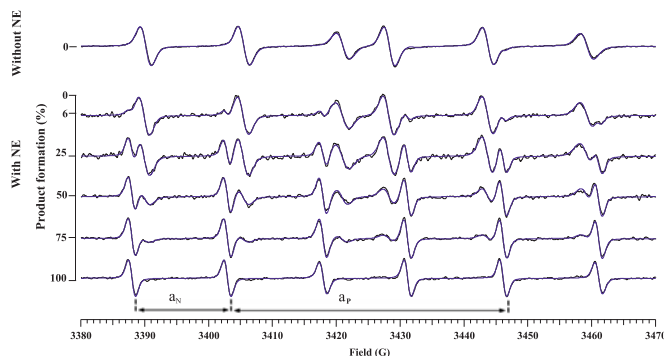


Fig. 1. EPR spectroscopy of the line-shifting nitroxide: hydrolysis of 40 μ M substrate **R-3** by 0.8 nM protease NE yielding the product **R-1**. Five EPR spectra are represented corresponding to five reaction steps: 6%, 25%, 50%, 75% and 100% of product formation. Only 6% of product was formed after the first EPR acquisition. Spectrum without NE corresponds to substrate **R-3** (0% of product) whereas spectrum with NE at 100% illustrates the product **R-1**. Spectra (dark lines) are fitted by a linear combination of substrate and product (blue lines). Hyperfine coupling of the unpaired electron with the phosphorus atom ^{31}P (spin $\frac{1}{2}$) and with the nitrogen atom ^{14}N (spin 1) provide 6 EPR lines. Parameters a_P and a_N are phosphorus and nitrogen coupling constants deduced from EPR product or substrate spectra. (For interpretation of the references to color in this figure legend, the reader is referred to the web version of this article.)

Table 1

EPR parameters of substrate and product. (a) Landé's factor (b) peak to peak linewidth of the fourth line. Enzymatic reaction induces a change in the phosphorus hyperfine coupling constant (a_P) hence creating a shift of the EPR lines. This shift can be used to measure an enzyme activity by EPR *in vitro* or to create contrast *in vivo* by OMRI. The parameters were measured in HEPES buffer 50 mM at pH 7.4, 0.15 M NaCl and Igepal 0.05%.

Nitroxides	a_N (G)	a_P (G)	$g^{(a)}$	Linewidths (G) ^(b)
Substrate	15.5	38.4	2.0052	1.84
Product	14.9	43.3	2.0053	1.22

3.2.3. Specificity screening of the substrate

Enzyme specificity screening was carried out *in vitro*. Initial velocities of product formation for various enzymes are shown in Fig. 4.

Of the proteases of different classes tested, only Neutrophil Elastase, Proteinase 3 and Porcine pancreatic elastase were able to hydrolyze the substrate into product at a significant rate. This narrow specificity is similar to that observed for the paranitroanilide-based analogous substrate. As NE and Proteinase 3 are two inflammation markers released from neutrophils by various means including degranulation [36,37], this substrate is very promising for the study of pulmonary inflammatory diseases. As expected for an elastase with similar substrate preferences, Porcine Pancreatic Elastase (PPE) was also able to catalyze

substrate hydrolysis at a high rate of the same order of magnitude as NE. Again, the selectivity of the peptide-linked nitroxide is similar to the one of the paranitroanilide chromogenic substrate bearing the same peptide. It is however irrelevant in the context of most inflammation diseases since PPE is synthesized as an inactive pro-enzyme and activated only in the intestinal lumen. Thus, the simultaneous presence of both enzymes is impossible except in pancreatitis where premature activation of PPE coexists with a strong inflammation. These experiments yielded similar results for isomers S and R.

3.2.4. Relevance to inflamed lung situations

To determine the relevance of this substrate for *in vivo* imaging of inflammation, NE detection was carried out using bronchoalveolar lavages derived from a mouse model of *Pseudomonas* pneumonia characterized by an acute pulmonary inflammation. Mice were *intra nasally* challenged with sterile PBS or containing *Pseudomonas aeruginosa* [21]. To assess the accuracy and specificity of NE detection, mice deficient in NE (NE-KO) or the three serine proteases namely NE, Proteinase 3 and Cathepsin G (3KO) were employed along with their Wild Type littermates (WT) [3]. Initial velocities were recorded by EPR after adding 1 mM substrate directly in the BronchoAlveolar Lavages (BALs) (Fig. 5).

As expected, infected WT mice BALs contained the maximal enzymatic activity. Interestingly, the activity in infected NE-KO mice samples dropped by 50% compared to the infected WT samples. Furthermore, 3KO lost 70% of the reference activity. Since Cathepsin G is inactive and Proteinase 3 active on this substrate, this additional activity decrease in 3KO can be confidently attributed to the absence of Proteinase 3. All control mice displayed an activity in the range of that corresponding to the control spontaneous dissociation. To further support our findings, prior addition of Batimastat, a broad spectrum matrix metalloproteinase inhibitor to infected BALs had no effect on activity measurements (data not shown). Thus, the detected activity stems exclusively from the neutrophil proteases NE and to a lesser extent from Proteinase 3. The apparent difference between the infected and uninfected 3KO samples is not statistically significant in this set of experiments. The slightly higher values for the infected 3KO could nevertheless be easily explained by some minor enzyme activities brought by the bacteria *Pseudomonas*. *Pseudomonas* elastase, however, cannot contribute as seen in Fig. 4.

Clearly, enzymatic activities in the setting of tissue inflammation can be detected by EPR in infected mouse BALs with this substrate. Significantly, hydrolysis of this substrate is due to active neutrophil proteases and hence represents a selective marker of inflammation.

3.3. Images of elastase activity using Overhauser-enhanced MRI

Recently, the discovery of nitroxide-based substrates undergoing strong electronic resonance spectrum alteration upon enzyme action led to the concept of "Overhauser switch" [17,18]. Overhauser-enhanced imaging was proven possible *in vitro* and *in vivo*. Thus, the NE specific substrate was probed as a potential polarizing agent through *in vitro* and

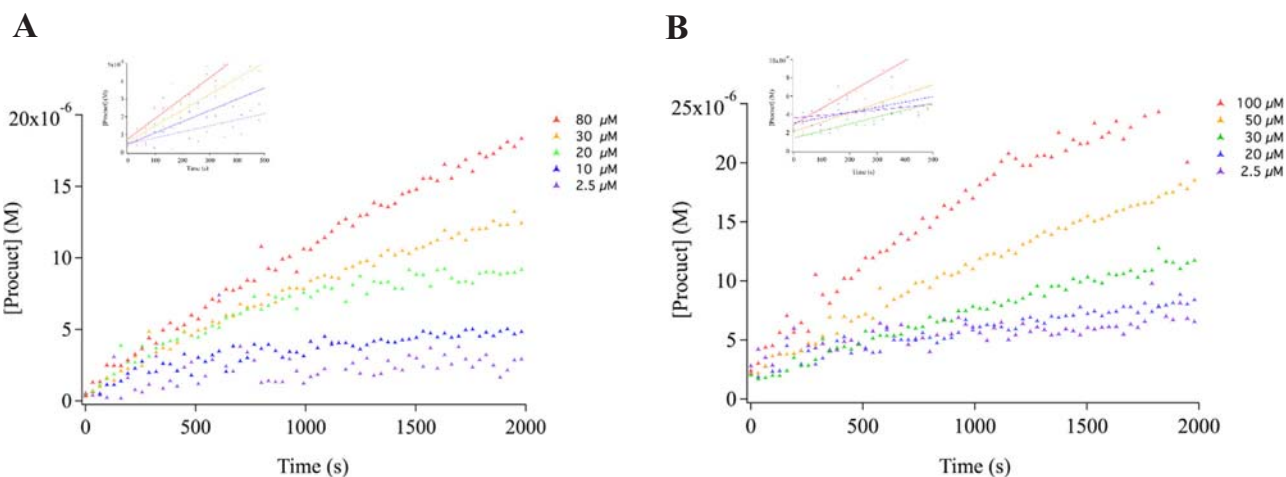


Fig. 2. Display of selected curves among those used for the calculation of the initial rate of product formation for a range of substrate concentration by 1 nM NE in HEPES buffer pH7.4 at 25 °C. A: isomer R; B: isomer S.

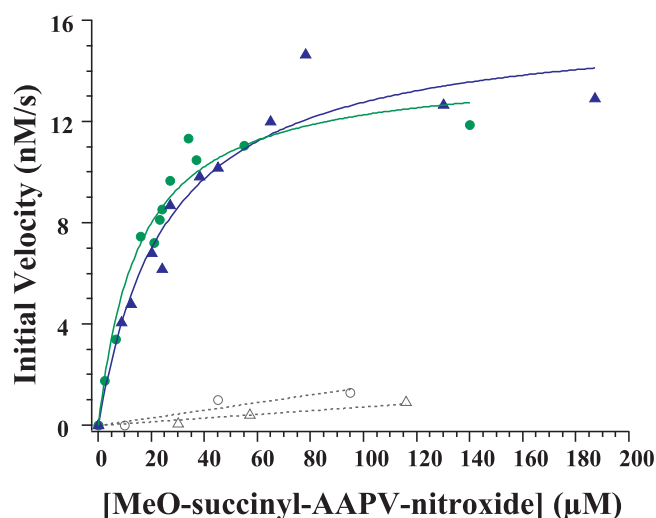


Fig. 3. Michaelis-Menten plot: initial velocities observed at different substrate concentrations (0–200 μM) in the presence of 1 nM NE. Both (R) and (S) substrate isomers are represented (blue triangles: isomer S and green circles: isomer R). Spontaneous dissociation for both isomers are also showed as dotted lines (open circles: Isomer R; open triangles: Isomer S). Both plots are fitted with the Michaelis-Menten equation (continuous lines). (For interpretation of the references to color in this figure legend, the reader is referred to the web version of this article.)

Table 2

Enzymatic Michaelis constants for the (R) and (S) substrate isomers.

	R-3•	S-3•
K_m (μM)	15 (± 2.9)	25 (± 5.4)
k_{cat} (s ⁻¹)	14 (± 0.9)	16 (± 1.1)
k_{cat}/K_m (s ⁻¹ M ⁻¹)	930,000	640,000

ex vivo OMRI experiments.

3.3.1. Properties of the substrate and the product as an OMRI contrast agent

The EPR irradiation frequency of the fourth line upfield was swept by tuning the cavity of the OMRI setup and the resulting MRI signal was plotted. The maximum signal enhancements were observed at distinct electronic EPR frequencies: 5425.6 MHz for the substrates **R-3•** or **S-3•** and 5414.4 MHz for the product **1•** (Fig. 6) as predicted from the EPR spectra.

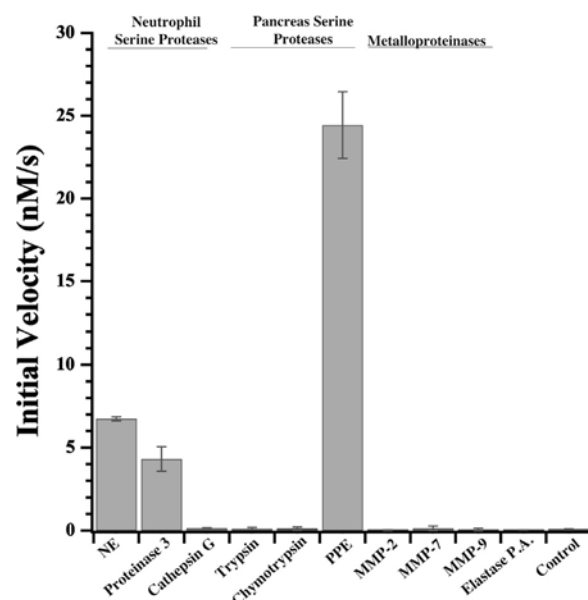


Fig. 4. EPR comparative kinetics of the nitroxide substrate isomer **S** hydrolysis by 9 different proteases. Kinetics of hydrolysis of 1 mM substrate was studied by EPR at 25 °C with 1 nM of each enzyme: NE, Proteinase 3, Cathepsin G, Trypsin, Chymotrypsin, PPE, MMP-2, MMP-7, MMP-9 and the metallo-elastase from *Pseudomonas Aeruginosa* (P.A). Substrate spontaneous dissociation in HEPES buffer is also represented as a control. Experiments were done in duplicate. Error bars represent the two limit values.

As for the EPR spectrometry study (cf. *Enzymatic hydrolysis of the substrate*), both lines are well separated and do not overlap. Linewidths are narrow enough to easily observe high signal enhancement in OMRI experiments. The full width at half maximum of the OMRI-derived EPR spectra in Fig. 6 was 7.4 MHz for the substrate **R-3•** and 4 MHz for the product **1•**. Thus, linewidths in OMRI data agree with the results obtained by EPR spectrometry. Difference in linewidth values could be explained by the difference in the molecular weight of each nitroxide form (cleaved or uncleaved) as it acts on the tumbling rate and a probable contribution of the conformational change that is expected to modify the hyperfine coupling with the cycle and methyl protons. Moreover, it can be noticed that the product EPR signal amplitude increased about 1.5 times upon hydrolysis thus facilitating proteolysis detection.

As the frequency domain of EPR irradiation in this OMRI experiment is narrow compared to the linewidths, each nitroxide can thus be

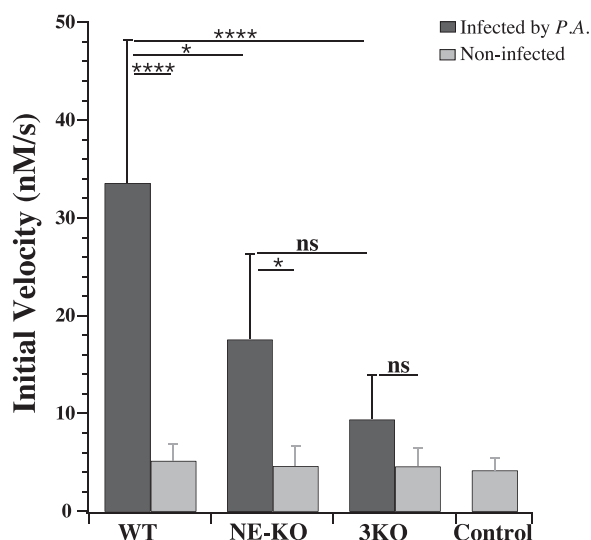


Fig. 5. Rate of product formation in bronchoalveolar lavages from unchallenged mice and mice infected by *Pseudomonas aeruginosa* (P.A.) for 24 h. 1 mM substrate was added extemporaneously. WT: wild type mice; NE-KO: mice Knocked-out for NE; 3KO: mice knocked-out for three neutrophil proteases. Control: spontaneous hydrolysis of the substrate. Significance bars are the result of an ordinary one-way ANOVA Tukey's multiple comparisons test.

observed selectively with specific irradiation. On one hand, irradiating a sample with the product EPR frequency will give access to the enzymatic activity. On the other hand, irradiating at the EPR frequency of the substrate will give access to its bio distribution.

The ^1H longitudinal relaxivity r_1 was measured through a classical MRI experiment for the substrate **3**• and the product **1**• and were equal to $0.40 \text{ s}^{-1}\text{mM}^{-1}$ and $0.42 \text{ s}^{-1}\text{mM}^{-1}$, respectively. Those results are comparable to the relaxivity r_1 of Oxo-TEMPO ($0.5 \text{ s}^{-1}\text{mM}^{-1}$) (unpublished results) which is characteristic of a water accessible electron.

The OMRI sensitivity at 0.2 T was investigated (Fig. 7). Maximum DNP factors reached -26 for the product at about 2 mM, and -6 for the substrate at about 1.4 mM. It should be noted that enhancement is higher for the product. This discrepancy might be the consequence of a lower EPR saturation efficacy of the substrate EPR line, since the electronic saturation is correlated to the nitroxide linewidth.

Interestingly, a DNP factor of -3 corresponding to an Overhauser enhancement of 2 (or to 200% contrast) remains for 0.09 mM of product (as inferred from Eq. (1) in the Material and methods section), which is a concentration compatible with future *in vivo* experiments. This result showed a very good sensitivity of the method as low substrate and product concentrations can be detected with high contrast.

3.3.2. Enzyme kinetics by OMRI *in vitro*

Since the substrate and the product can be detected by OMRI enzyme activity imaging was probed. Hence, the substrate was reacted with neutrophil elastase and the hydrolysis was monitored by OMRI. Fig. 8 shows relevant images acquired with the EPR irradiation set at the product or the substrate frequency as a function of time.

A maximum Overhauser enhancement of 5 for the substrate was obtained at the beginning of the reaction whereas a maximum enhancement of 8 for the product was obtained at the end of the reaction. The estimated catalytic constant by OMRI using the initial slope of the time-resolved Michaelis kinetics ($k_{\text{cat}} = 6 \text{ s}^{-1}$) revealed a similar value than the one calculated by EPR (see Table 2). Thus this substrate is suitable for the detection neutrophil elastase activity by Overhauser-enhanced Magnetic Resonance Imaging. It is also an imaging method suitable to visualize the bio distribution of the substrate.

4. Discussion

Molecular imaging of enzyme activity by MRI is a long-sought-after tool. To achieve this, it was needed to produce a contrast and to trigger it specifically *via* enzyme activity. Since enzyme concentrations are mostly in the nanomolar range an amplification step was also necessary to overcome the gap of sensitivity with MRI which essentially produces images from the highly concentrated water protons. In this study high contrast was given by Overhauser-enhanced MRI in the presence of a nitroxide. The contrast was conditioned to enzyme catalysis by linking a specific peptide to a line-shifting nitroxide. Thus by choosing the EPR irradiating frequency of the “Overhauser switch” either the substrate or the product (hence the enzyme activity) would produce contrast. Furthermore, signal amplification naturally occurred from the enzyme turn-over as long as fresh substrate was present. The first approach was to target Neutrophil Elastase, a protease associated with numerous inflammatory diseases. After characterization, the substrate was successfully tested on samples from a *Pseudomonas aeruginosa* lungs infection.

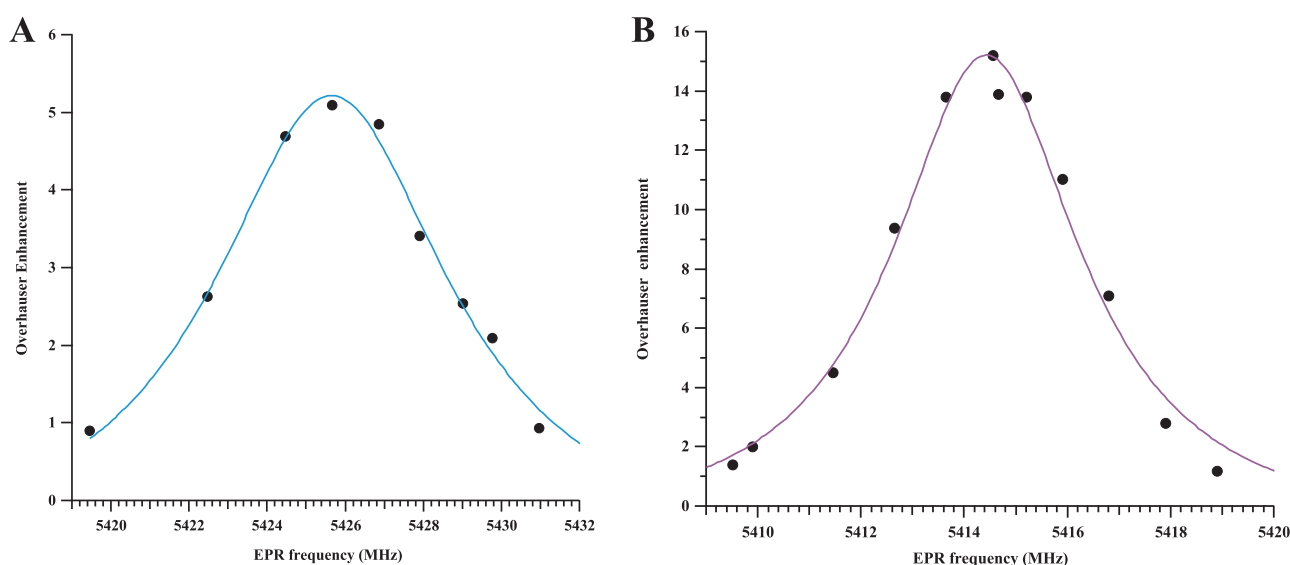


Fig. 6. Determination of the optimal excitation EPR frequencies for OMRI experiments: The EPR irradiation frequency of the fourth line upfield was swept and the resulting MRI signal was plotted. Overhauser signal enhancement of the substrate **R-3**• (A) and product **1**• (B) were fitted using a Lorentzian model. The MRI B_0 field was 0.1936 T for the substrate and 0.1935 T for the product.

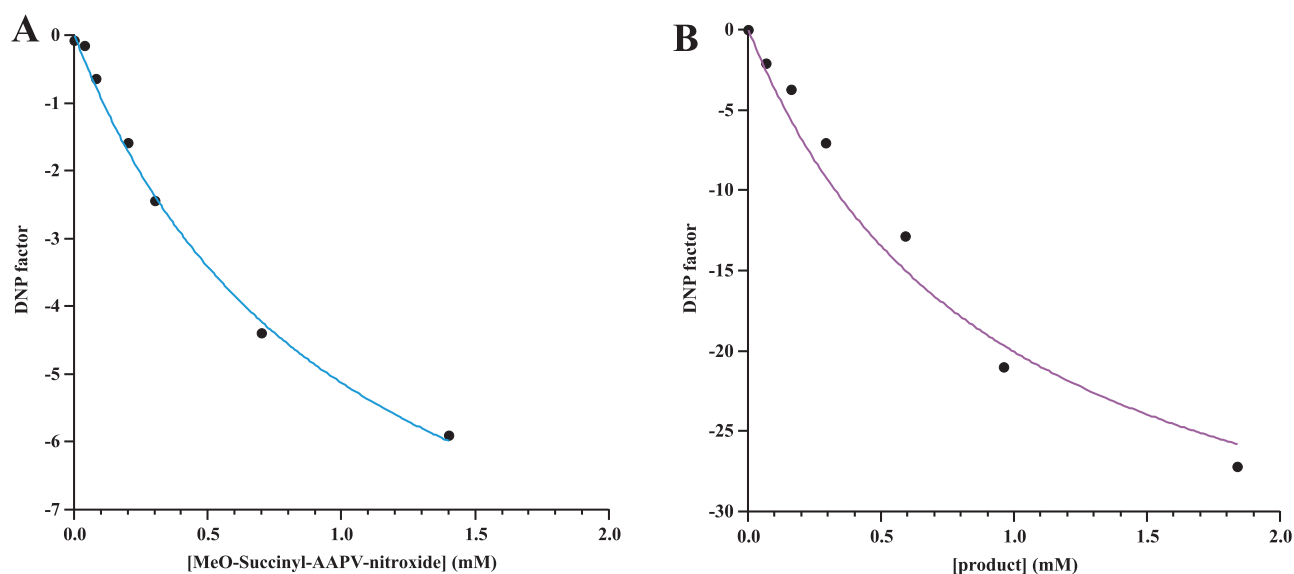


Fig. 7. DNP factor as a function of nitroxide concentration. A: Substrate **3•** (Parameters: Saturation factor $s = 0.25$; coupling factor $\rho = 0.36$; relaxivity $r_1 = 0.4 / \text{s/mM}$); B : Product **1•** (Parameters : Saturation factor $s = 1$, coupling factor $\rho = 0.36$; relaxivity $r_1 = 0.42 / \text{s/mM}$).

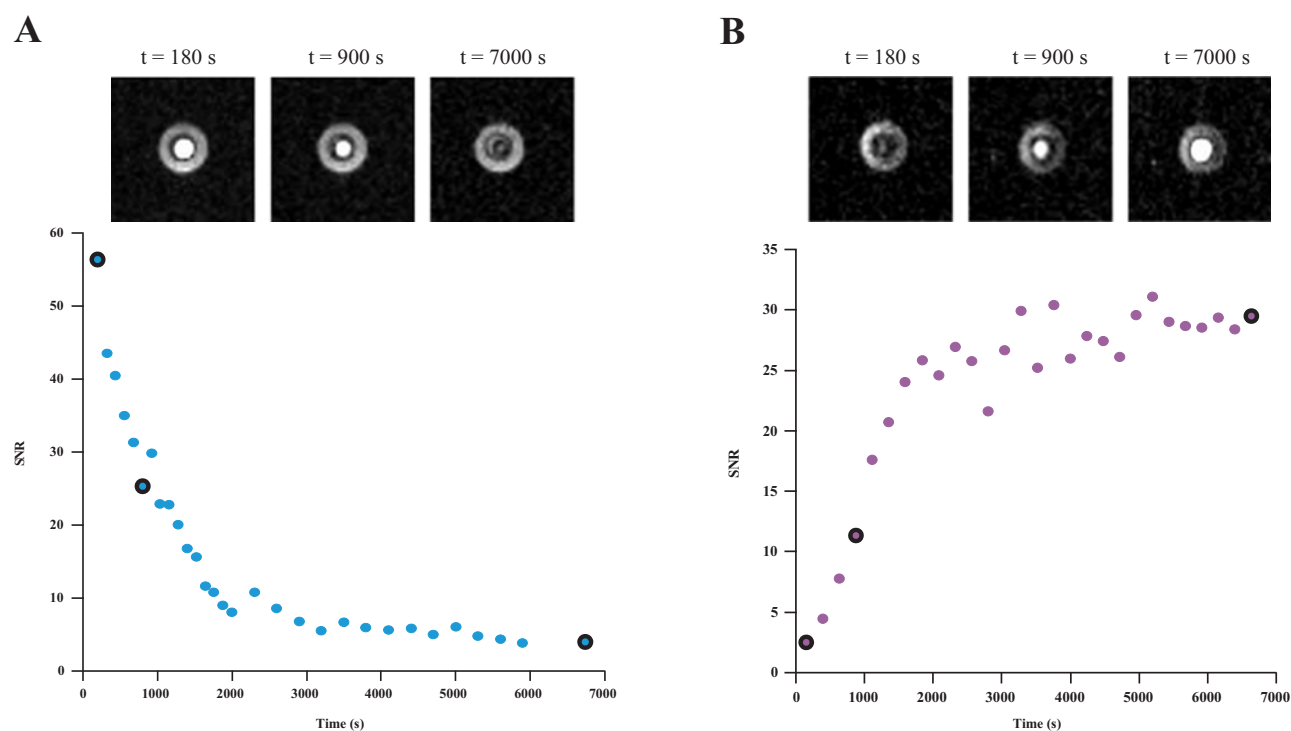


Fig. 8. OMRI monitoring of substrate consumption and product formation from elastase proteolysis. A: 2D images selected from the corresponding time course (highlighted points) of substrate consumption. The initial substrate concentration was 1 mM and the proteolytic reaction was accelerated by adding 20 nM enzyme. The EPR frequency was tuned at 5426 MHz. B: 2D images selected from the corresponding time course (highlighted points) of product formation. The initial substrate concentration was 0.5 mM and enzyme concentration was 40 nM. The EPR frequency was tuned at 5415 MHz.

The difficult but successful grafting of a chosen peptide on the shifting nitroxide core suggests that a new family of protease activity probe can be designed. Furthermore, the acetate enol ester [18] and the elastase-specific peptide enol ester have the same EPR spectrum and yield the same product after hydrolysis. Thus, the same instruments and the same settings will be valid regardless of the protease targeted. Expanding the targeted proteases by varying the peptide would allow exploring other pathologies like pancreatitis or tumors via their associated specific protease activity.

4.1. The MeO-Suc-(Ala)₂-Pro-Val-nitroxide is a specific and fast substrate for elastase.

The specificity tests show that MeO-Suc-(Ala)₂-Pro-Val-nitroxide is a fast substrate for Neutrophil Elastase and in a lesser extent for Proteinase 3. All other tested proteinases including serine proteinases and matrix metallo proteinases are ineffective. Particularly, the metallo elastase from *Pseudomonas aeruginosa* does not generate any product. Thus, with the irrelevant exception of pancreatic elastase, this substrate is a reliable marker of inflammation via neutrophil serine proteases. The

Michaelis constants for elastase reveal a better substrate than its optically active paranitroanilide analog. In mouse BALs from the present acute inflammation model an activity from 1 nM of NE is detected. In human, BALs are estimated to dilute the epithelial lining fluid of about one hundred fold [38]. Thus, the concentration of NE in lungs of wild type infected mice would be 100 nM *in vivo*. In this situation, using the Michaelis constants, a concentration as low as 75 μ M of substrate (5 times the K_m) would generate 1.4 μ M/s of product which would thus reach 140 μ M in 100 s. Such a product concentration generates an OMRI contrast of 200% as deduced from the OMRI sensitivity plot. *In vivo* imaging of acute inflammation should then be possible within a short time provided that the substrate could be supplied quickly to the lungs prior to OMRI. In the case of cystic fibrosis concentrations of active elastase in the epithelial lining fluid are in the range of 2 μ M even for patients with mild lung disease [39]. This is 2000 fold the lower limit of our method thus ensuring a fast and strong signal in a few seconds.

4.2. Towards a new tool first for research then for diagnosis

The first expected impact of this study is to provide a useful and very specific diagnostic tool for inflamed lungs. More specifically, the goal is to perform molecular MRI of any protease/inhibitor imbalance with a true 3D resolution firstly for Neutrophil Elastase but also Cathepsin G, Proteinase 3, MMP-12 and marginally for NSP4. It would then be possible to inventory the endangered areas in the lungs and later verify that a protective treatment with protease inhibitors has indeed inhibited the enzyme activity. This diagnosis at a molecular scale could be done prior to any anatomical alteration. Abnormal proteolysis would be visible thus at a much earlier stage of the disease when lung can still be preserved. For instance, in the *Pseudomonas aeruginosa* infection model it was possible to monitor the inflammation while the lungs were reversibly altered. Ultimately it could be used as a monitoring tool for a personalized treatment until protease activity is effectively inhibited. All images were performed using the same setup as for *in vivo* imaging of mice published earlier. Thus, at shorter term, the method could be used as a pre-clinical tool to develop protease inhibition strategies for emphysema or cystic fibrosis using animal experimental models with a real-time monitoring of protease activity inhibition *in vivo*. To this end, studies are ongoing.

New diagnosis on human could be done using the presented nitroxide substrate and EPR. For instance, since EPR is able to perform on samples that are opaque to the visible light it could be used to detect enzyme activity in tissue samples such as biopsies.

All OMRI experiments herein validated the use of the substrate MeO-Suc-(Ala)₂-Pro-Val-nitroxide as a specific proteolysis probe for OMRI. Future *in vivo* experiments of proteolysis imaging will be done to visualize pulmonary inflammation *in situ*. Application to human diagnosis with OMRI will require further development. This stems from the EPR frequency that is about 650 times higher than NMR frequency. Consequently, at 0.2 T the electron resonance frequency is in the microwave range around 5.4 GHz. While it is possible to make mouse images this frequency is not suitable for larger animals because of low penetration depth. Interestingly, MRI at very low field is a currently active research area [40–44]. For instance at earth magnetic field the EPR frequency of nitroxides is in the range of several dozens of MHz, which allows convenient saturation of electron states and high penetration depths suitable for humans.

Acknowledgments

This study was achieved within the context of the ANR PULMOZYME (ANR-15-CE18-0012-01) and the Cluster of Excellence TRAIL ANR-10-LABX-57. The authors thank Aix-Marseille University for A*MIDEX grant (ANR-11-IDEX-0001-02) funded by the Investissements d'Avenir French Government program, managed by

the French National Research Agency (ANR). ID is grateful for the funding from the People Program (Marie Curie Actions) of the European Union's Seventh Framework Program (FP7/2007–2013) under REA grant agreement no. PCOFUND-GA-2013-609102, through the PRESTIGE program coordinated by Campus France. We also thank “Fonds Agir pour les Maladies Chroniques”, Rhône Alpes Auvergne.

- [1] J.B. Soriano, A.A. Abajobir, K.H. Abate, S.F. Abera, A. Agrawal, M.B. Ahmed, et al., Global, regional, and national deaths, prevalence, disability-adjusted life years, and years lived with disability for chronic obstructive pulmonary disease and asthma, 1990–2015: a systematic analysis for the Global Burden of Disease Study 2015, *GBD 2015 Chronic Respiratory Disease Collaborators*, *Lancet Respir. Med.* 5 (9) (2017) 691–706, [https://doi.org/10.1016/S2213-2600\(17\)30293-X](https://doi.org/10.1016/S2213-2600(17)30293-X) Epub 2017 Aug 16. Erratum in: *Lancet Respir. Med.* 2017 Oct;5(10):e30.PMID:28822787.
- [2] B. Korkmaz, M.S. Horwitz, D.E. Jenne, F. Gauthier, Neutrophil elastase, proteinase 3, and cathepsin G as therapeutic targets in human diseases, *Pharmacol. Rev.* 62 (4) (2010) 726–759, <https://doi.org/10.1124/pr.110.002733> (PubMed PMID: 21079042; PubMed Central PMCID: PMC2993259).
- [3] N. Guyot, J. Wartelle, L. Malleret, A.A. Todorov, G. Devouassoux, Y. Pacheco, et al., Unopposed cathepsin G, neutrophil elastase, and proteinase 3 cause severe lung damage and emphysema, *Am. J. Pathol.* 184 (8) (2014) 2197–2210, <https://doi.org/10.1016/j.ajpath.2014.04.015> (PubMed PMID: 24929239).
- [4] C. Boudier, P. Laurent, J.G. Bieth, Leukoproteases and pulmonary emphysema: cathepsin G and other chymotrypsin-like proteinases enhance the elastolytic activity of elastase on lung elastin, *Adv. Exp. Med. Biol.* 167 (1984) 313–317 (PubMed PMID: 6369910).
- [5] K.A. Serban, D.N. Petrusca, A. Mikosz, C. Poirier, A.D. Lockett, L. Saint, et al., Alpha-1 antitrypsin supplementation improves alveolar macrophages efferocytosis and phagocytosis following cigarette smoke exposure, *PLoS One* 12 (4) (2017) e0176073, <https://doi.org/10.1371/journal.pone.0176073> (PubMed PMID: 28448535; PubMed Central PMCID: PMC5407578).
- [6] I. Schechter, A. Berger, On the size of the active site in proteases. I. Papain, *Biochem. Biophys. Res. Commun.* 27 (2) (1967) 157–162 (PubMed PMID: 6035483).
- [7] S. Matsumoto, H. Yasui, S. Batra, Y. Kinoshita, M. Bernardo, J.P. Munasinghe, et al., Simultaneous imaging of tumor oxygenation and microvascular permeability using Overhauser enhanced MRI, *Proc. Natl. Acad. Sci. USA* 106 (42) (2009) 17898–17903, <https://doi.org/10.1073/pnas.0908447106> (PubMed PMID: 19815528; PubMed Central PMCID: PMC2761243).
- [8] J. Weaver, S.R. Burks, K.J. Liu, J.P. Kao, G.M. Rosen, In vivo EPR oximetry using an isotopically-substituted nitroxide: potential for quantitative measurement of tissue oxygen, *J. Magn. Reson.* 271 (2016) 68–74, <https://doi.org/10.1016/j.jmr.2016.08.006> (PubMed PMID: 27567323; PubMed Central PMCID: PMC5266518).
- [9] B. Epel, S.V. Sundramoorthy, M. Krzykawska-Serda, M.C. Maggio, M. Tseytlin, G.R. Eaton, et al., Imaging thiol redox status in murine tumors in vivo with rapid-scan electron paramagnetic resonance, *J. Magn. Reson.* 276 (2017) 31–36, <https://doi.org/10.1016/j.jmr.2016.12.015> (PubMed PMID: 28092786; PubMed Central PMCID: PMC5336491).
- [10] T. Kawano, M. Murata, F. Hyodo, H. Eto, N. Kosem, R. Nakata, et al., Noninvasive mapping of the redox status of dimethylnitrosamine-induced hepatic fibrosis using in vivo dynamic nuclear polarization-magnetic resonance imaging, *Sci. Rep.* 6 (2016) 32604, <https://doi.org/10.1038/srep32604> (PubMed PMID: 27587186; PubMed Central PMCID: PMC5009327).
- [11] I. Dhimitruka, A.A. Bobko, T.D. Eubank, D.A. Komarov, V.V. Khramtsov, Phosphonated trityl probes for concurrent in vivo tissue oxygen and pH monitoring using electron paramagnetic resonance-based techniques, *J. Am. Chem. Soc.* 135 (15) (2013) 5904–5910, <https://doi.org/10.1021/ja401572r> (PubMed PMID: 23517077; PubMed Central PMCID: PMC3982387).
- [12] J.-L. Clement, S. Barbat, C. Frejaville, A. Rockenbauer, P. Tordo, Synthesis and use as spin-trap of 5-methyl-5-phosphono-1-pyrroline N-oxide (DHPMPO). pH Dependence of the EPR parameters of the spin adducts, *J. Chem. Soc. Perkin Trans. 2* (9) (2001) 1471–1475, <https://doi.org/10.1039/B103830N>.
- [13] S. Thetiot-Laurent, G. Gosset, J.L. Clement, M. Cassien, A. Mercier, D. Siri, et al., New amino-acid-based beta-phosphorylated nitroxides for probing acidic pH in biological systems by EPR spectroscopy, *Chembiochem: Eur. J. Chem. Biol.* 18 (3) (2017) 300–315, <https://doi.org/10.1002/cbic.201600550> (PubMed PMID: 27885767).
- [14] W. Takahashi, A.A. Bobko, I. Dhimitruka, H. Hirata, J.L. Zweier, A. Samouilov, et al., Proton-electron double-resonance imaging of pH using phosphonated trityl

- probe, *Appl. Magn. Reson.* 45 (9) (2014) 817–826, <https://doi.org/10.1007/s00723-014-0570-2> (PubMed PMID: 25530673; PubMed Central PMCID: PMC4268155).
- [15] G. Audran, L. Bosco, P. Bremond, T. Butscher, S.R. Marque, Solvent effect in beta-phosphorylated nitroxides. Part 4: detection of traces of water by electron paramagnetic resonance, *Org. Biomol. Chem.* 14 (4) (2016) 1288–1292, <https://doi.org/10.1039/c5ob02316e> (PubMed PMID: 26647997).
- [16] E. Parzy, V. Bouchaud, P. Massot, P. Voisin, N. Koonjoo, D. Moncelet, et al., Overhauser-enhanced MRI of elastase activity from in vitro human neutrophil degranulation, *PLoS One* 8 (2) (2013) e57946, <https://doi.org/10.1371/journal.pone.0057946> (PubMed PMID: 23469112; PubMed Central PMCID: PMC3585236).
- [17] N. Koonjoo, E. Parzy, P. Massot, M. Lepetit-Coiffe, S.R. Marque, J.M. Franconi, et al., In vivo overhauser-enhanced MRI of proteolytic activity, *Contrast Media Mol. Imaging* 9 (5) (2014) 363–371, <https://doi.org/10.1002/cmmi.1586> (PubMed PMID: 24729587).
- [18] G. Audran, L. Bosco, P. Bremond, J.M. Franconi, N. Koonjoo, S.R. Marque, et al., Enzymatically shifting nitroxides for EPR spectroscopy and overhauser-enhanced magnetic resonance imaging, *Angew. Chem.* 54 (45) (2015) 13379–13384, <https://doi.org/10.1002/anie.201506267> (PubMed PMID: 26376730).
- [19] D.J. Lurie, I. Nicholson, J.R. Mallard, Low-field EPR measurements by field-cycled dynamic nuclear polarization, *J. Magn. Reson.* (1969) 95 (2) (1991) 405–409, [https://doi.org/10.1016/0022-2364\(91\)90230-Q](https://doi.org/10.1016/0022-2364(91)90230-Q).
- [20] P. Massot, E. Parzy, L. Pourtau, P. Mellet, G. Madelin, S. Marque, et al., In vivo high-resolution 3D overhauser-enhanced MRI in mice at 0.2 T, *Contrast Media Mol. Imaging* 7 (1) (2012) 45–50, <https://doi.org/10.1002/cmmi.464> (PubMed PMID: 22344879).
- [21] A. Belaouaj, R. McCarthy, M. Baumann, Z. Gao, T.J. Ley, S.N. Abraham, et al., Mice lacking neutrophil elastase reveal impaired host defense against gram negative bacterial sepsis, *Nat. Med.* 4 (5) (1998) 615–618 (PubMed PMID: 9585238).
- [22] D.M. MacIvor, S.D. Shapiro, C.T. Pham, A. Belaouaj, S.N. Abraham, T.J. Ley, Normal neutrophil function in cathepsin G-deficient mice, *Blood* 94 (12) (1999) 4282–4293 (PubMed PMID: 10590073).
- [23] K. Kessenbrock, L. Fröhlich, M. Sixt, T. Lammernann, H. Pfister, A. Bateman, et al., Proteinase 3 and neutrophil elastase enhance inflammation in mice by inactivating antiinflammatory progranulin, *J. Clin. Invest.* 118 (7) (2008) 2438–2447, <https://doi.org/10.1172/JCI34694> (PubMed PMID: 18568075; PubMed Central PMCID: PMC2430496).
- [24] Y. Tamura, S. Suzuki, T. Sawada, Role of elastase as a virulence factor in experimental *Pseudomonas aeruginosa* infection in mice, *Microb. Pathog.* 12 (3) (1992) 237–244 (PubMed PMID: 1614334).
- [25] R. Boxio, J. Wartelle, B. Nawrocki-Raby, B. Lagrange, L. Malleret, T. Hirche, et al., Neutrophil elastase cleaves epithelial cadherin in acutely injured lung epithelium, *Respir. Res.* 17 (1) (2016) 129, <https://doi.org/10.1186/s12931-016-0449-x> (PubMed PMID: 27751187; PubMed Central PMCID: PMC5067913).
- [26] S.D. Shapiro, N.M. Goldstein, A.M. Houghton, D.K. Kobayashi, D. Kelley, A. Belaouaj, Neutrophil elastase contributes to cigarette smoke-induced emphysema in mice, *Am. J. Pathol.* 163 (6) (2003) 2329–2335, [https://doi.org/10.1016/S0002-9440\(10\)63589-4](https://doi.org/10.1016/S0002-9440(10)63589-4) (PubMed PMID: 14633606; PubMed Central PMCID: PMC1892384).
- [27] P. Mellet, P. Massot, G. Madelin, S.R. Marque, E. Harte, J.M. Franconi, et al., New concepts in molecular imaging: non-invasive MRI spotting of proteolysis using an Overhauser effect switch, *PLoS One* 4 (4) (2009) e5244, <https://doi.org/10.1371/journal.pone.0005244> (PubMed PMID: 19396361; PubMed Central PMCID: PMC2671144).
- [28] A.W. Overhauser, Polarization of nuclei in metals, *Phys. Rev.* 92 (2) (1953) 411–415.
- [29] A. Abragam, J. Combrisson, I. Solomon, *Compt. Rend. Acad. Sci. Paris* 245 (1957) 157.
- [30] R.L. Vold, J.S. Waugh, M.P. Klein, D.E. Phelps, Measurement of spin relaxation in complex systems, *J. Chem. Phys.* 48 (8) (1968) 3831–3832, <https://doi.org/10.1063/1.1669699>.
- [31] N.J. Indraniil Duttagupta, G.érard Audran, Jean-Michel Franconi, Sylvain R.A. Marque, Philippe Massot, Philippe Mellet, Elodie Parzy, Eric Thiaudière, Nicolas Vanthuyne, Selective on/off-nitroxides as radical probes to investigate nonradical enzymatic activity by electron paramagnetic resonance, *Chem. Eur. J.* (2018), <https://doi.org/10.1002/chem.201800866> (In press).
- [32] B. McKeever, G. Pattenden, Total synthesis of trunkamide A, a novel thiazoline-based prenylated cyclopeptide metabolite from *Lissoclinum* sp, *Tetrahedron* 59 (15) (2003) 2713–2727, [https://doi.org/10.1016/S0040-4020\(03\)00294-1](https://doi.org/10.1016/S0040-4020(03)00294-1).
- [33] I. Duttagupta, D. Misra, S. Bhunya, A. Paul, S. Sinha, Cis–trans conformational analysis of 8-azaproline in peptides, *J. Org. Chem.* 80 (21) (2015) 10585–10604, <https://doi.org/10.1021/acs.joc.5b01668>.
- [34] R. Rajagopalan, R.R. Kuntz, U. Sharma, W.A. Volkert, R.S. Pandurangi, Chemistry of bifunctional photoprobes. 6. Synthesis and characterization of high specific activity metalated photochemical probes: development of novel rhenium photoconjugates of human serum albumin and fab fragments, *J. Org. Chem.* 67 (19) (2002) 6748–6757 (PubMed PMID: 12227807).
- [35] C. Koehl, C.G. Knight, J.G. Bieth, Compared action of neutrophil proteinase 3 and elastase on model substrates. Favorable effect of S'-P' interactions on proteinase 3 catalysts, *J. Biol. Chem.* 278 (15) (2003) 12609–12612, <https://doi.org/10.1074/jbc.M210074200> (PubMed PMID: 12538645).
- [36] K. Ohlsson, I. Olsson, The extracellular release of granulocyte collagenase and elastase during phagocytosis and inflammatory processes, *Scand. J. Haematol.* 19 (2) (1977) 145–152 (PubMed PMID: 197589).
- [37] C.T. Pham, Neutrophil serine proteases: specific regulators of inflammation, *Nat. Rev. Immunol.* 6 (7) (2006) 541–550, <https://doi.org/10.1038/nri1841> (PubMed PMID: 16799473).
- [38] S.I. Rennard, G. Basset, D. Lecossier, K.M. O'Donnell, P. Pinkston, P.G. Martin, et al., Estimation of volume of epithelial lining fluid recovered by lavage using urea as marker of dilution, *J. Appl. Physiol.* 60 (2) (1986) 532–538 (PubMed PMID: 3512509).
- [39] M.W. Konstan, K.A. Hilliard, T.M. Norvell, M. Berger, Bronchoalveolar lavage findings in cystic fibrosis patients with stable, clinically mild lung disease suggest ongoing infection and inflammation, *Am. J. Respir. Crit. Care Med.* 150 (2) (1994) 448–454, <https://doi.org/10.1164/ajrccm.150.2.8049828> (PubMed PMID: 8049828).
- [40] M. Sarraçanie, C.D. LaPierre, N. Salameh, D.E. Waddington, T. Witzel, M.S. Rosen, Low-cost high-performance MRI, *Sci. Rep.* 5 (2015) 15177, <https://doi.org/10.1038/srep15177> (PubMed PMID: 26469756; PubMed Central PMCID: PMC4606787).
- [41] V.S. Zotev, T. Owens, A.N. Matlashov, I.M. Savukov, J.J. Gomez, M.A. Espy, Microtesla MRI with dynamic nuclear polarization, *J. Magn. Reson.* 207 (1) (2010) 78–88, <https://doi.org/10.1016/j.jmr.2010.08.015> (PubMed PMID: 20843715; PubMed Central PMCID: PMC2956831).
- [42] D. Grucker, In vivo detection of injected free radicals by overhauser effect imaging, *Magn. Reson. Med.* 14 (1) (1990) 140–147 (PubMed PMID: 2161981).
- [43] P.J. Ross, L.M. Broche, D.J. Lurie, Rapid field-cycling MRI using fast spin-echo, *Magn. Reson. Med.* 73 (3) (2015) 1120–1124, <https://doi.org/10.1002/mrm.25233> (PubMed PMID: 24753306).
- [44] D.E.J. Waddington, M. Sarraçanie, H. Zhang, N. Salameh, D.R. Glenn, E. Rej, et al., Nanodiamond-enhanced MRI via in situ hyperpolarization, *Nat. Commun.* 8 (2017) 15118, <https://doi.org/10.1038/ncomms15118> (PubMed PMID: 28443626; PubMed Central PMCID: PMC5414045).